Simulation of the charge transport across grain boundaries in *p*-type $SrTiO_3$ ceramics under dc load: Debye relaxation and dc bias dependence of long-term conductivity

Th. Hölbling
Institut fuer Werkstoffe der Elektrotechnik, University of Technology Aachen, D-52056 Aachen, Germany

R. Waser
Institut fuer Werkstoffe der Elektrotechnik, University of Technology Aachen, D-52056 Aachen, Germany and IFF/EKM, Research Center Juelich, D-52425 Juelich, Germany

(Received 19 October 2001; accepted for publication 10 December 2001)

A mathematical-physical model to describe the charge transport across grain boundaries in *p*-type $SrTiO_3$ ceramics in the low-temperature regime for arbitrary dc voltage steps has been developed. The finite element model structure consists of a one-dimensional cross section through a ceramic scenario. Mathematical formulation comprises a coupled system of continuity equations (utilizing Maxwell-Boltzmann transport equations) and Poisson's equation, with the appropriate boundary conditions for a potentiostatic simulation approach. The edges of the model are assumed to be blocking for ionic transport, and penetrable for electronic transport. The model was implemented exploiting routines from the numerical class library DIFFPACK™. After an initial electrostatic simulation a dc bias voltage step is applied. The evolution of the spatial profiles of electric potential, defect concentrations, space-charge density, and electric conductivity, and the current response are calculated. The results for the ceramic model structure confirm the experimentally observed Debye relaxation, and the characteristic dependence of long-term conductivity on the dc bias after space-charge polarization, before the onset of resistance degradation. © *2002 American Institute of Physics.* [DOI: 10.1063/1.1448404]

I. INTRODUCTION

Perovskite-type titanate ceramics are used in ceramic multilayer capacitors (in the following referred to as CMCs) due to their high dielectric permittivity. There is a sustaining trend towards further miniaturization for those devices. Along this trend, the thickness of the dielectric layer in CMCs is decreasing. Hence, for unaltered operating voltages in electronic circuits, dc field stress increases. This leads to an enhanced leakage current through the device. This component-related problem is the motivation for theoretically investigating leakage current behavior in perovskite-type titanates.

As model material, *p*-type $SrTiO_3$ has been chosen, since it reveals a defect and crystal structure that is very similar to that of $BaTiO_3$, which is still the most important ceramic material in the capacitor industry. In contrast, $SrTiO_3$ is not ferroelectric over the complete temperature range of technical interest. For modeling purposes, this is advantageous since the ferroelectric behavior imposes an additional degree of complexity by significantly affecting the polarization and charge transport in the material.

Leakage current behavior is immediately related to charge transport across grain boundary (GB) barriers. The GB barrier effect is well known and extensively studied for *n*-type semiconducting ceramics to which both the varistor and the positive temperature coefficient (PTC) effect are ascribed.[1–5] In both cases, the scenario of negatively charged GB states compensated by positively charged donor centers in the bulk adjacent to the GBs, forming a space-charge depletion layer, is assumed. From an electronic view, the GBs can be described as a back-to-back double Schottky barrier.

For *p*-type oxides that are subject of this article, the GB effect is less well understood. Investigations on doped oxygen ion conductors such as CeO_2[6–9] and ZrO_2,[10–13] because of their technical applications as solid electrolytes in high-temperature fuel cells, reveal a discrepancy between the crystallographic thickness and the electric thickness of the highly resistive GB layer. This supports the model of the formation of a space-charge depletion layer at GBs, just as in *n*-type ceramics.

For the mixed-conducting Perovskite-type alkaline-earth titanates such as *p*-type $SrTiO_3$, highly resistive GB layers were observed by impedance spectroscopy in the time and frequency domain.[14–18] A corresponding Schottky-type space-charge depletion layer model was suggested by Waser,[19] and Chiang and Takagi.[20]

Further research of charge transport phenomena on the basis of the Schottky depletion model focused on *p*-type $SrTiO_3$.[21–23] Hagenbeck developed a simulation tool based on a suggestion of one of the authors for the GB scenario and the well-understood bulk defect chemistry for *p*-type $SrTiO_3$ (Ref. 24) to calculate the spatial profiles of the defect concentrations and the electric potential at GBs for the electrostatic equilibrium case.[25–27] Impedance spectra simulation that were derived from the electrostatics calculation for the small-signal (Ohmic) regime matched excellently with experimental data,[28] thus confirming the applicability of the GB Schottky depletion model. Simulation of chemical diffu-

 © 2002 American Institute of Physics

Downloaded 15 Dec 2006 to 134.94.122.39. Redistribution subject to AIP license or copyright, see http://jap.aip.org/jap/copyright.jsp

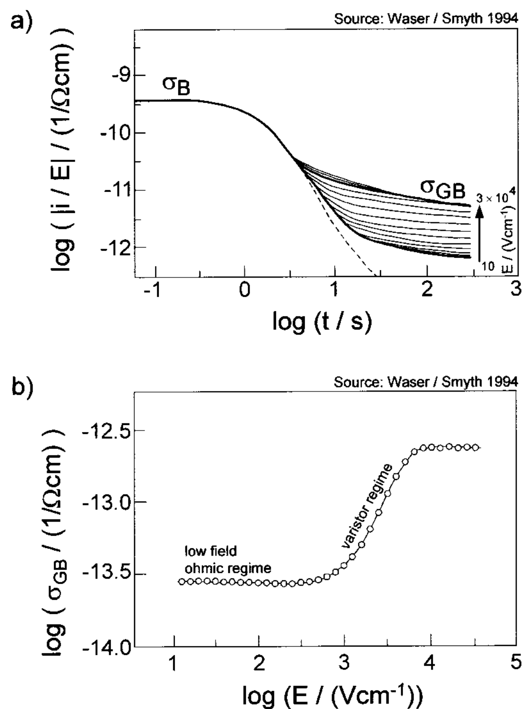

FIG. 1. (a) Typical current response (here as geometry-independent electric conductivity) of p-type $SrTiO_3$ for different dc bias voltage steps (external electric field E) in the low-temperature regime. Short-term conductivity is ascribed to the bulk (σ_B), and long-term conductivity is ascribed to the GBs (σ_{GB}). (b) Dependence of σ_{GB} on the dc bias (graphs taken from Ref. 21).

sion through GB interfaces,[29–31] and the influence of the geometric orientation of GBs on the impedance spectra,[32,33] in the small-signal regime, and highly resolved impedance measurement on individual GBs,[34,35] were performed recently by the research group of Maier.

In this article, a mathematical-physical simulation model to describe charge transport phenomena in p-type $SrTiO_3$ ceramics for arbitrary dc bias voltage steps in the low-temperature regime is introduced. The model focuses on the time dependence of the current response, the dependence of long-term conductivity on the dc bias, and the spatial distribution of the electric potential and the defect concentrations in the depletion layer at GBs and the adjacent undisturbed bulk regions.

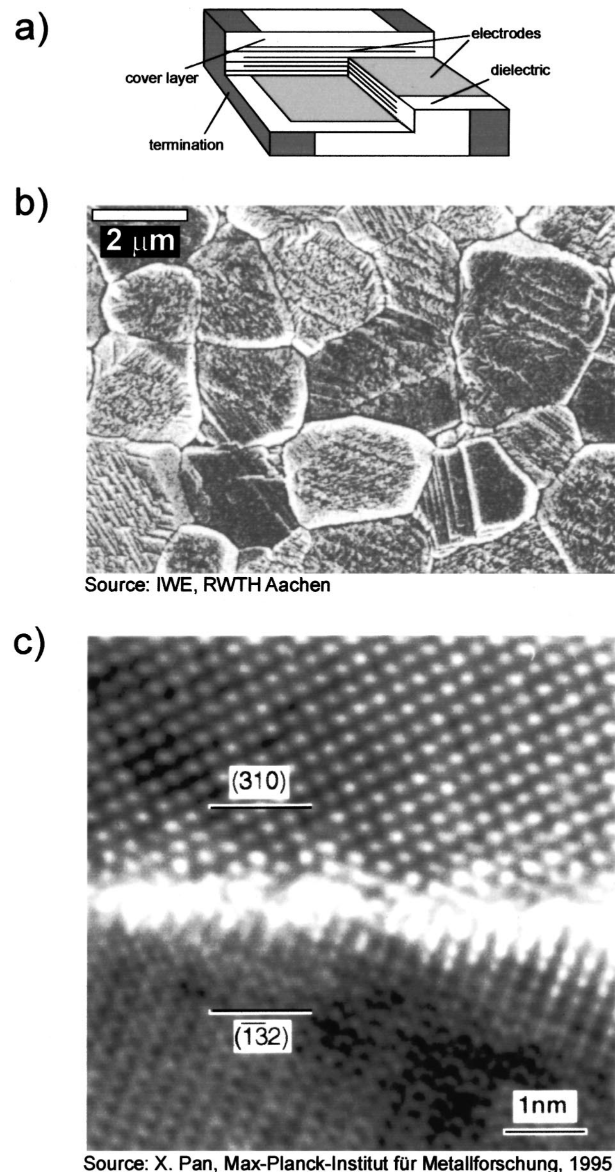

FIG. 2. (a) Sketch of a ceramic multiplayer capacitor (b) scanning electron microscopy picture of a p-type $SrTiO_3$ ceramic with an average grain size of 2 μm (c) high-resolution transmission electron microscopy picture of a grain boundary in a p-type $SrTiO_3$ ceramic. The width of the crystallographic mismatch zone is about 1 nm.

II. EXPERIMENT

p-type $SrTiO_3$ ceramics reveal a characteristic current behavior after a dc bias voltage step before the onset of resistance degradation[36] (Fig. 1). The current response [in Fig. 1(a)] displayed as geometry-independent ratio of the absolute values of electric current density i and external electric field E (i.e., electric conductivity) reveals Debye-type relaxation characteristics due to material phases of different conductivity in the bulk and at the grain boundary space-charge layer. This leads to space-charge polarization at the GBs. Short-term conductivity before relaxation is ascribed to the bulk (σ_B), and long-term conductivity (i.e., leakage current) is ascribed to the GBs (σ_{GB}).

Whereas σ_B, and for not too large biases the relaxation time, are independent of the dc bias, σ_{GB} depends significantly upon the dc bias. There are three characteristic regimes of σ_{GB} [Fig. 1(b)]. For low voltages, an Ohmic regime is observed, with constant σ_{GB}. It is followed by a varistor regime where σ_{GB} increases strongly within a bias voltage range of about one order of magnitude. For even larger biases, σ_{GB} reaches saturation.

III. MICROSTRUCTURE AND POINT DEFECTS

In p-type $SrTiO_3$ polycrystals [Fig. 2(b)], for a wide range of oxygen partial pressures during equilibration, in the low-temperature regime (LT, $T<700$ K) one finds a characteristic constellation of point defects in the bulk [Fig. 3(a)]. In the following, Kröger-Vink notation[37] will be used to identify the point defects.

Downloaded 15 Dec 2006 to 134.94.122.39. Redistribution subject to AIP license or copyright, see http://jap.aip.org/jap/copyright.jsp

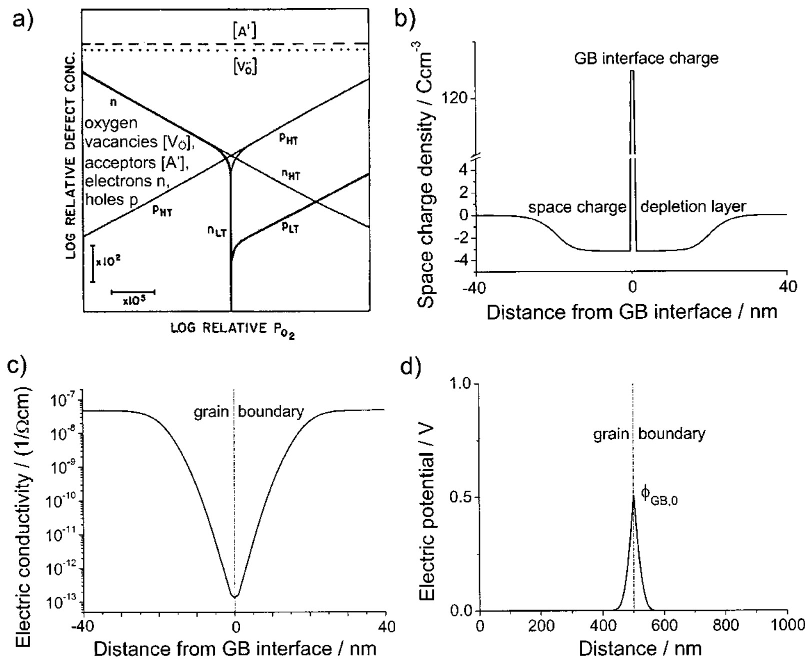

FIG. 3. (a) Bulk point defect concentrations in p-type $SrTiO_3$ as a function of the oxygen partial pressure p_{O_2} during equilibration, for low temperatures (LT, $T < 700$ K), and high temperatures (HT). At low temperatures and high p_{O_2}, the relation $n \ll p \ll [A'] \cong 2[V_O^{\cdot\cdot}]$ is valid. (b) Spatial simulation of the Schottky-type space charge depletion layer at GBs in p-type $SrTiO_3$ for the electrostatic equilibrium scenario. (c) Simulated conductivity profile corresponding to (b). (d) Simulated spatial profile of the electric potential corresponding to (b).

After sintering, due to impurities and doping, an amount of negatively charged acceptors A' is found.[38–40] The incorporation of acceptors is accompanied by the formation of positively charged doubly ionized oxygen vacancies $V_O^{\cdot\cdot}$, the charge of the latter compensating the acceptor charge for the sake of electroneutrality. For temperatures $T > 700$ K equilibrium with the ambient gas phase is maintained, leading to oxidation or reduction of the material. In oxidizing atmospheres, oxygen vacancies are partially filled from the ambient, with the creation of electron holes. This mechanism is described by the reaction

$$V_O^{\cdot\cdot} + \frac{1}{2}O_2 \rightleftharpoons O_O + 2h^{\cdot}, \tag{1}$$

where $h^{\cdot}$ denotes the electron holes, O_O the oxygen atoms on regular lattice sites, and O_2 atmospheric oxygen. Eventually, due to Eq. (1), holes are established as the majority charge carriers for electronic conduction, as regarded in this work. In the low-temperature regime $T < 700$ K, the surface reaction according to Eq. (1) is obstructed. Thus, the overall concentration of oxygen vacancies can be regarded as "frozen-in."[41,42] The concentration of holes $[h^{\cdot}]$ (usually referred to as p) is much lower than concentration of oxygen vacancies $[V_O^{\cdot\cdot}]$ and acceptors $[A']$, whereas the concentration of the electrons n is much lower than p. Altogether, the relation between the defect concentrations $[A'] \cong 2[V_O^{\cdot\cdot}] \gg p \gg n$ applies in the bulk of p-type $SrTiO_3$ for the above-mentioned temperature and partial pressure regime.

In the low-temperature regime, only the $V_O^{\cdot\cdot}$ and the electronic charge carriers are considered mobile in p-type $SrTiO_3$.[43–47] Even though $[V_O^{\cdot\cdot}]$ exceeds p by many orders of magnitude, the holes do contribute significantly to electric conductivity σ due to their mobility that is by many orders of magnitude higher than that of oxygen vacancies. On the other hand, the contribution of the electrons to σ is negligible due to their low concentration, despite their high mobility.

In p-type $SrTiO_3$ one finds crystallographically "sharp" GBs (no second phases)[48] with a width of the interface mismatch area of about 1 nm [Fig. 2(c)]. For the scenario at GBs, one of the authors proposed a model of additional, positively charged donor states that occur at the GB interface:[19] due to Coulombic repulsion, the adjacent bulk regions are depleted of the mobile holes and $V_O^{\cdot\cdot}$. The remaining negatively charged acceptor ions are shaping a Schottky-type space-charge layer that compensates the GB donor charge for the sake of global electro-neutrality [Fig. 3(b)]. Due to depletion of mobile charge carriers, electric conductivity within the space-charge layer is greatly reduced with respect to the undisturbed bulk [Fig. 3(c)].

This space-charge layer forms an internal potential barrier $\varphi_{GB,0}$ [Fig. 3(d)] given by

$$\varphi_{GB,0} = \frac{Q_{GB}^2}{8\varepsilon_0 \varepsilon_r q_0 [A']} \tag{2}$$

with Q_{GB} denoting the charge density of the GB donor states, ε_0 the permittivity of free space, ε_r the relative dielectric permittivity, and q_0 the unit charge.

Under applied bias, this barrier hampers the transport of the positively charged mobile carriers across GBs. The spatial profiles of physical quantities at GBs displayed in Figs. 3(b)–3(d) were simulated according to Hagenbeck.[25]

In the small-signal (Ohmic) regime, the concentration profiles from the electrostatics calculation can be exploited for impedance spectra simulation.[28] Yet, for sufficiently high bias voltages, the defect chemical scenario, due to shift of point defect concentrations, changes drastically with respect to the electrostatic case.[23] Thus, for higher bias voltages, charge transport phenomena may not be derived from electrostatics calculations any longer; moreover, local changes of defect concentration due to charge transport must be considered. A suitable model is introduced in the following section.

Downloaded 15 Dec 2006 to 134.94.122.39. Redistribution subject to AIP license or copyright, see http://jap.aip.org/jap/copyright.jsp

IV. MODELING

A finite element model for charge transport in p-type $SrTiO_3$ in the low-temperature regime was developed. The ceramic structure is modeled as a one-dimensional cross section through polycrystalline p-type $SrTiO_3$ that is bounded on the edges by flat-band electrodes (no initial band bending in the electrostatic case). In this approach it is assumed that highly conducting paths along GBs, i.e., due to inversion layers at the interface,[28,49] do not exist. The material is shaped as a continuous medium, disregarding the periodical atomic lattice structure of the perovskite and allowing the use of macroscopic quantities such as ε_r to describe the physical scenario.

Energy levels following the band diagram are assigned to the electronic and ionic defects to describe the defect chemical reactions in the material. All mobile and immobile material defects are modeled as spatial profiles of particle concentrations throughout the finite element mesh. The finite element mesh is nonuniform, since a higher spatial resolution is chosen for critical material areas where large gradients of the physical quantities are expected [i.e., electrodes, space-charge depletion area, GB interface, Fig. 4(a)]. To obtain startup values for the simulation under dc bias, an initial electrostatics calculation is performed (for further details see Refs. 26, 27, 49).

To describe particle transport, the validity of the Maxwell-Boltzmann transport equations is assumed. Accordingly, the local particle current density of the mobile species i, $j_i(x)$, is described as the sum of a drift component, $j_{\mathrm{Drift},i}(x)$, due to a local electric field $E(x)$, and a diffusion component, $j_{\mathrm{Diff},i}(x)$, due to a local gradient of the concentration of the species, $c_i(x)$ [a thermal contribution to $j_i(x)$ is neglected, assuming the absence of a temperature gradient within the material]. This gives

$$j_i(x)=j_{\mathrm{Drift},i}(x)+j_{\mathrm{Diff},i}(x) \tag{3}$$

with

$$j_{\mathrm{Drift},i}(x)=\left(\frac{1}{z_i q_0}\right)\mu_i c_i(x)E(x) \tag{4}$$

and

$$j_{\mathrm{Diff},i}(x)=-D_i\frac{\partial c_i(x)}{\partial x} \tag{5}$$

with μ_i denoting the mobility, D_i the diffusion coefficient, and z_i the charge number of the species i. Mobility and diffusion coefficient are coupled via the Nernst-Einstein relation $\mu_i=kT/|z_i|q_0 D_i$. k denotes the Boltzmann constant, and T the temperature in the material. The electric current density of the species i, $i_i(t)$, is obtained by multiplying the current density according to Eq. (3) with the charge of the species, yielding

$$i_i(t)=j_i(t)z_i q_0. \tag{6}$$

For the total electric current density $i_{\mathrm{tot}}(t)$ the sum of all partial electric current density, and a displacement current component $\dot{D}=(1/\varepsilon)\ (\partial E/\partial t)$, must be considered, yielding

$$i_{\mathrm{tot}}(t)=\sum_i i_i(t)+\dot{D}. \tag{7}$$

The local change of the defect concentration of the species i is described by continuity equations

$$\frac{\partial c_i(x)}{\partial t}=-\nabla\vec{j}_i(x)+q_i(x) \tag{8}$$

with $q_i(x)$ denoting an additional source term, e.g., due to defect chemical reactions. Due to the low mobility of electronic charge carriers in p-type $SrTiO_3$ with respect to semiconductor materials, thus the short mean free path, it is assumed that there will always be local electronic equilibrium throughout the model.[23] This implies the validity of the relation $np=\mathrm{const}$ for the concentration of the electronic charge carriers. Thus, the source terms in Eq. (8) can be neglected, and description of transport of electronic charge carriers can be limited to one single continuity equation for the holes.

The coupling of the electric potential $\varphi(x)$ and the concentration of charged species is described by Poisson's equation:

a)

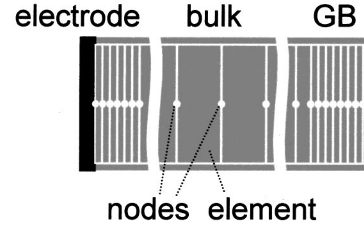

b)

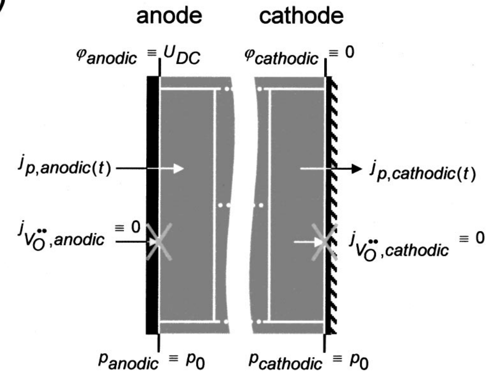

FIG. 4. (a) Scheme of the finite element mesh laid upon the model geometry for the simulation of charge transport across GBs in p-type $SrTiO_3$. The model equations are solved at each node of the mesh. For critical areas, e.g., where large gradients of the system state quantities are assumed (GB interfaces, electrodes), a high spatial resolution, i.e., density of nodes, is chosen, whereas noncritical areas are resolved more coarsely, leading to a nonuniform mesh. (b) Scheme of the scenario at the boundaries of the model structure for the simulation of charge transport across GBs in p-type $SrTiO_3$. Time-independent boundary conditions are formulated at the cathode (subscript: cathodic) and the anode (subscript: anodic) for the oxygen vacancy partial current density $j_{V_O^{\cdot\cdot}}$, the hole concentration p, and the electric potential φ. The oxygen vacancies may not pass the electrodes, so that, other than the partial current density $j_p(t)$ of the holes, $j_{V_O^{\cdot\cdot}}$ vanishes at the boundaries. φ_{anodic} is the dc bias voltage U_{dc}, $\varphi_{cathodic}$ equals zero. p_{anodic} and $p_{cathodic}$ are set at the electrostatic equilibrium bulk concentration p_0.

Downloaded 15 Dec 2006 to 134.94.122.39. Redistribution subject to AIP license or copyright, see http://jap.aip.org/jap/copyright.jsp

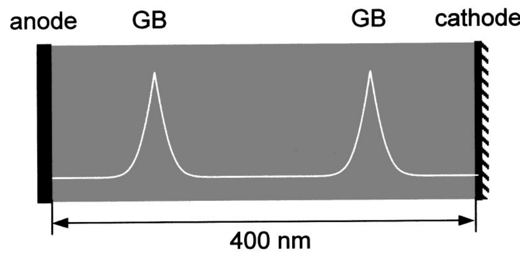

FIG. 5. Sketch of the model geometry for the simulation of large-signal charge transport across GBs in p-type $SrTiO_3$. It consists of a 400 nm one-dimensional longitudinal cut through a ceramic model structure which contains two GB interfaces, each at a distance of 100 nm from the electrode, with adjacent bulk regions. The model geometry is assumed to be bounded by "flat-band" electrodes on either side. The potential distribution in the geometry for the electrostatic case is hinted at by the white line. It is assumed that no highly conducting inversion layers at the GBs exist which in a real ceramic structure would "short circuit" the current path across GBs.

$$\frac{\partial^2 \varphi(x)}{\partial x^2} = -\frac{\rho(x)}{\varepsilon} \tag{9}$$

with the local space charge density $\rho(x)=q_0\Sigma_i z_i c_i(x)$ as the local sum of all charged species, and the dielectric permittivity $\varepsilon=\varepsilon_0\varepsilon_r$.

The scenario at the model boundaries is displayed in Fig. 4(b). For the edges of the model structure, constant values of the electric potential are assumed. By the choice of those boundary values, a dc bias voltage step U_{dc} is imposed on the model, with $\varphi_{anodic}=U_{dc}$ at the anode, and $\varphi_{cathodic}=0$ at the cathode. The hole concentration at both electrodes is "pinned" and set at the bulk equilibrium value obtained by the initial electrostatic calculation p_0 (flat-band scenario). The electrodes are penetrable for the electronic charge carriers (partial current density j_p).

Since the total amount of oxygen vacancies in the material can be regarded as constant with time (see previous section), oxygen vacancies can neither enter nor leave the material. This is modeled by boundary conditions for the partial current density of the oxygen vacancies $j_{V_O^{\cdot\cdot}}$ that vanishes on the edges of the model geometry. Hence, under the influence of an external bias, the oxygen vacancies can only redistribute between anode and cathode.

The model was implemented utilizing routines from the numerical class library DIFFPACK™. At the nodes of the finite element mesh in Fig. 4(a) exact solution of the model equations (8) and (9) are obtained. For details on the modeling and numeric aspects of the simulation see Refs. 50, 51. Further results will be published elsewhere.[52]

V. SIMULATION RESULTS

A. Space-charge polarization (Debye relaxation)

To study the current response $i_{tot}(t)$ and its contributions in p-type $SrTiO_3$ ceramics under high-field stress, a dc voltage step simulation was performed utilizing a model structure according to Fig. 5, consisting of two grain boundary interfaces "embedded" in a bulk area between anode and cathode. A bulk acceptor concentration of $N_A=2\times10^{19}\ \mathrm{cm}^{-3}$ and a GB donor concentration of $N_{D,GB}=1.75\times10^{21}\ \mathrm{cm}^{-3}$ are assumed; the temperature is $T=500$ K, with a relative dielectric permittivity of $\varepsilon_r=150$, mobility of oxygen vacancies $\mu_{V_O^{\cdot\cdot}}=10^{-8}\ \mathrm{cm^2/Vs}$,[43,46] and holes $\mu_p=0.5\ \mathrm{cm^2/Vs}$.[44] The dc bias is $U_{dc}=8$ V. The simulation results are presented in Fig. 6(a).

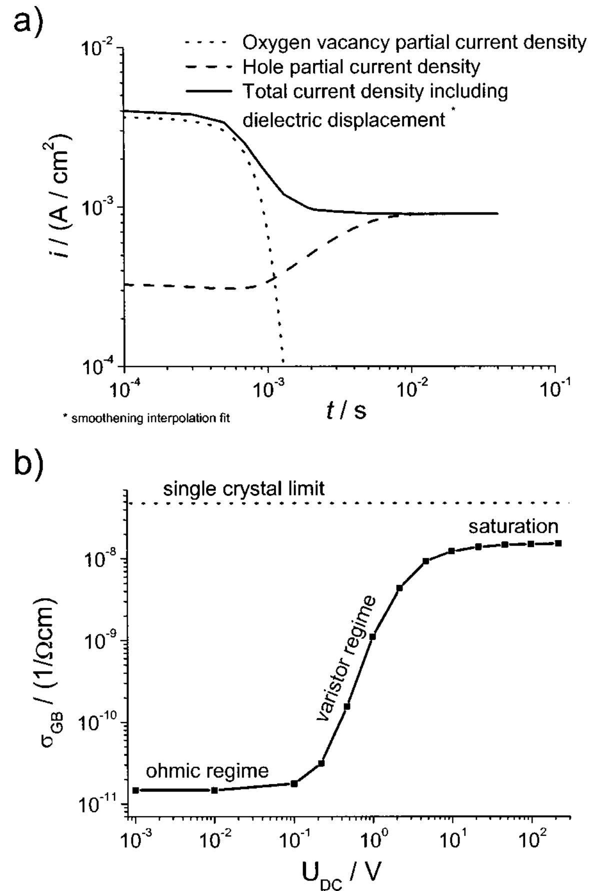

FIG. 6. Simulation results for a p-type $SrTiO_3$ ceramic model structure (Fig. 5) after a large-signal dc bias voltage step in the low-temperature regime ($T=500$ K) (a) Total current response and its contributions. (b) dc bias voltage dependence of long-term conductivity σ_{GB}.

For short times, the total current consists of both electronic (hole) and ionic ($V_O^{\cdot\cdot}$) contributions. After Debye relaxation (space-charge polarization) the ionic contribution to the current has vanished. Thus, in the stationary state before resistance degradation, the current is completely electronic (hole type).

Hence, the $V_O^{\cdot\cdot}$ will no longer contribute to dc electric conductivity. Thus, long-term electric conductivity is completely determined by the spatial profile of the hole concentration in the space-charge depletion layer at the GBs [Fig. 7(c)].

B. dc bias dependence of long-term conductivity

To investigate the dependence of the long-term electrical conductivity σ_{GB} on the dc bias in p-type $SrTiO_3$ ceramics, a model structure different from the one used for the simulation of the current response in the time domain is chosen. Since σ_{GB} is ascribed to the GBs, it is desired to exclude the influence of the voltage drop across space-charge depletion layers at the electrodes. In a real ceramic with a large number

Downloaded 15 Dec 2006 to 134.94.122.39. Redistribution subject to AIP license or copyright, see http://jap.aip.org/jap/copyright.jsp

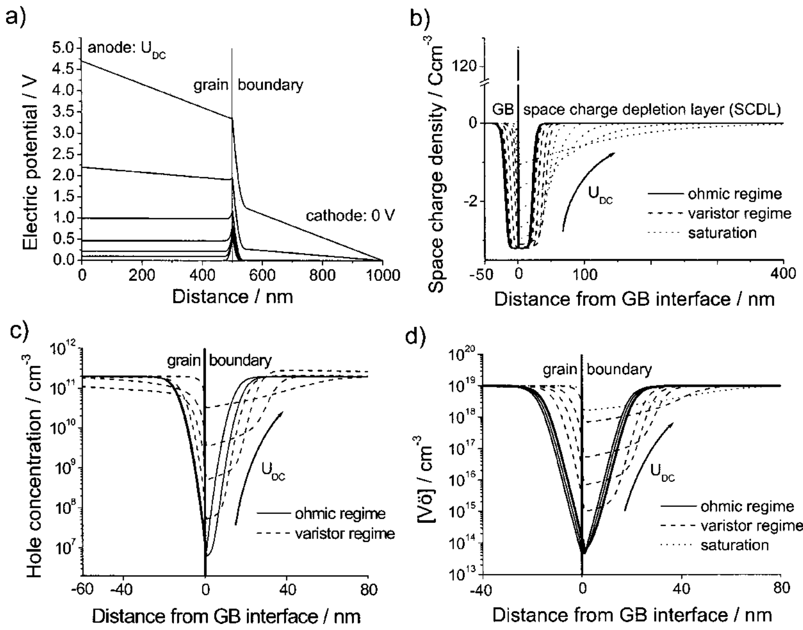

FIG. 7. Simulated spatial profiles of (a) the electric potential $\varphi(x)$, (b) the space-charge density $\rho(x)$, (c) the hole concentration $p(x)$, and (d) the oxygen vacancy concentration $[V_O^{\cdot\cdot}](x)$ for a p-type $SrTiO_3$ bicrystal at $T=500$ K, in the stationary state after space-charge polarization at various dc bias voltages.

of GBs along a one-dimensional cross section from anode to cathode the influence of the electrodes can be neglected.[21] Yet, due to numerical restrictions, an extended ceramic may not be modeled. Thus, for focusing at the influence of the GBs on charge transport only, a bicrystal model structure as an excerpt from a real ceramic far from the edges (electrodes) is considered. The width of the bicrystal is 1 μm. By this approach, the dc bias drops exclusively across the bicrystal GB. Hence, the influence of the electrodes will be driven to zero. This simplification was justified by Hagenbeck's simulation approach whose calculations for a bicrystal model structure did match excellently with measurement data from experiments on extended ceramics with a large number of GBs.[28] The simulation falls into two steps: First the redistribution of oxygen vacancies for the stationary state under dc bias is calculated, with "open" boundaries for their transport, according to the above-stated assumption for the bicrystal model. As stated earlier, $V_O^{\cdot\cdot}$ does not contribute to long-term dc conductivity σ_{GB}. Second, the concentration profile of the holes $p(x)$ for the stationary state is calculated, based on the altered space-charge density scenario at the GB due to the redistribution of the $V_O^{\cdot\cdot}$. From $p(x)$, σ_{GB} emerges by averaging the local conductivities throughout the model, neglecting capacitive contributions due to the complete decay of displacement current in the stationary state [see Fig. 6(a)].

The simulation was performed assuming a bulk acceptor concentration of $N_A=2\times10^{19}$ cm^{-3} and a GB donor concentration of $N_{D,GB}=8\times10^{20}$ cm^{-3}. Temperature is $T=500$ K, with a relative dielectric permittivity of $\varepsilon_r=150$, mobility of oxygen vacancies $\mu_{V_O^{\cdot\cdot}}=10^{-8}$ cm^2/Vs, and holes $\mu_p=0.5$ cm^2/Vs, just as for the current response simulation. dc bias voltage U_{dc} ranges from 1 mV to 220 V.

The simulation results for the dependence of long-term conductivity σ_{GB} on U_{dc} after redistribution of the $V_O^{\cdot\cdot}$ reveal the experimentally observed three regimes [see Fig. 6(b)]. They depend on the relation between U_{dc} and the intrinsic potential barrier at GBs for $U_{dc}=0$ (electrostatic scenario), $\varphi_{GB,0}$ [see Eq. (2)]. The corresponding spatial profiles of the electric potential $\varphi(x)$, the space-charge density $\rho(x)$, and the concentration of holes $p(x)$ and oxygen vacancies $[V_O^{\cdot\cdot}](x)$ for different values of U_{dc} in the stationary state are presented in Fig. 7.

For small biases ($U_{dc}\ll\varphi_{GB,0}$) the voltage completely drops across the GB [Fig. 7(a)]; the bulk regions adjacent to the space-charge depletion layer (in the following abbreviated as SCDL) remain field free, and the potential barrier at GBs φ_{GB} remains unchanged with respect to the electrostatic scenario. $p(x)$ [Fig. 7(c)] remain virtually unchanged as well. Thus, σ_{GB} remains constant.

Towards larger dc biases ($U_{dc}\approx\varphi_{GB,0}$), the positive charge carriers drift into the SCDL and across the GB interface to an increased extent. This leads to a pronounced increase of both $[V_O^{\cdot\cdot}]$ [Fig. 7(d)] and p [Fig. 7(c)] in the SCDL, the latter leading to a strong increase of σ_{GB} within a moderate range of U_{dc}. Moreover, U_{dc} drops across the bulk area outside the space-charge layer at an increased amount [Fig. 7(a)]. The SCDL shifts from the anode to the cathode [Fig. 7(b)]. Since the relation $p\ll[V_O^{\cdot\cdot}]$ is valid throughout the material, the contribution of the holes to space charge is negligible. Thus, the shift of $\rho(x)$ can be attributed to the redistribution of $V_O^{\cdot\cdot}$. Correspondingly, φ_{GB} is subsequently decreasing to zero which is inline with Schottky diffusion theory (see also Ref. 22):

$$\varphi_{GB}(U_{GB})=\varphi_{GB,0}\cdot\left(1-\frac{U_{GB}}{4\varphi_{GB,0}}\right)^2 \tag{10}$$

with U_{GB} denoting the voltage drop over a GB. As long as the voltage drop across the bulk is small with respect to U_{GB}, the relation $U_{GB}\approx U_{dc}$ applies for the model structure. According to Eq. (10), with the above-stated input parameters for the simulation, φ_{GB} will have vanished at a bias voltage of ≈2 V. This is in good agreement with the simulation results displayed in Fig. 7(a).

Downloaded 15 Dec 2006 to 134.94.122.39. Redistribution subject to AIP license or copyright, see http://jap.aip.org/jap/copyright.jsp

As long as in the SCDL $[V_O^{\cdot\cdot}]$ remains much smaller than the concentration of ionized acceptors $[A']$, the original shape of the SCDL is maintained [Fig. 7(b)]. Since its extension d_{GB} determines the GB capacity C_{GB} and, hence, Debye relaxation time τ_R, the independence of the latter of the dc bias for not too large biases is confirmed as well.[28] Whereas this is inline with results for p-type CeO_2 ceramics,[9] it is in contradiction to results for n-type ZnO varistors where a change of d_{GB} is predicted even at small biases.[53]

Towards even higher voltages ($U_{dc} \gg \varphi_{GB,0}$) the anodic side of the space-charge layer vanishes completely due to $V_O^{\cdot\cdot}$ drift. When $[V_O^{\cdot\cdot}]$ in the SCDL comes into the range of the acceptor concentration $[A']$ [Fig. 7(d)], the shape of the SCDL distorts [Fig. 7(b)]; to maintain global electroneutrality, $V_O^{\cdot\cdot}$ and holes are dragged away from the GBs to an increased extent, causing a pronounced depletion of formerly undisturbed bulk areas. This compensates the increase of p at the GBs. Hence, there is no further net increase of σ_{GB}. Moreover, the decrease of d_{GB} causes a decrease of the GB capacity, thus a decrease of τ_R. This was experimentally observed by Vollmann at very large bias.[54]

VI. CONCLUSIONS

(1) A mathematical-physical finite element model to simulate charge transport in p-type $SrTiO_3$ ceramics in the low-temperature regime for arbitrary dc voltage steps U_{dc} was developed. The simulation results for the ceramic model structure are in good agreement with experimental data.

(2) Space-charge polarization in the time domain due to the redistribution of the oxygen vacancies within the ceramic has been confirmed. The long-term current is purely electronic (p type). Thus, long-term conductivity σ_{GB} is exclusively determined by the spatial distribution of the hole concentration $p(x)$.

(3) The dependence of σ_{GB} on U_{dc} with its three characteristic regimes can be ascribed to the change of $p(x)$ with U_{dc} at the GB space-charge depletion layers.

(4) The decrease of Debye relaxation time τ_R at very high bias voltages is due to the increase of the GB space-charge depletion layer width d_{GB} that leads to a decrease of GB capacity C_{GB}, hence, of τ_R.

[1] G. E. Pike and C. H. Seager, Adv. Ceram. **1**, 53 (1980).
[2] F. Greuter, G. Blatter, M. Rossinelli, and F. Stucki, Ceram. Trans. **3**, 31 (1989).
[3] T. K. Gupta, J. Am. Ceram. Soc. **73**, 1817 (1990).
[4] J. Daniels and R. Wernicke, Philips Res. Rep. **31**, 544 (1976).
[5] J. Daniels, K. H. Härdtl, and R. Wernicke, Philips Tech. Rundsch. **38**, 1 (1979).
[6] D. Y. Wang and A. S. Nowick, J. Solid State Chem. **35**, 325 (1980).
[7] R. Gerhardt and A. S. Nowick, J. Am. Ceram. Soc. **69**, 641 (1986).
[8] R. Gerhardt and A. S. Nowick, J. Am. Ceram. Soc. **69**, 647 (1986).
[9] J. Tanaka, J. F. Baumard, and P. Abelard, J. Am. Ceram. Soc. **70**, 637 (1987).
[10] J. E. Bäuerle, J. Phys. Chem. Solids **30**, 2657 (1979).
[11] N. M. Beekmans and L. Heyne, Electrochim. Acta **21**, 303 (1976).
[12] M. Verkerk, B. J. Middelhuis, and A. J. Burggraaf, Solid State Ionics **6**, 159 (1982).
[13] B. C. H. Steele and E. P. Butler, Br. Ceram. Proc. **36**, 45 (1985).
[14] J. Maier, G. Schwitzgebel, and H. J. Hagemann, J. Solid State Chem. **58**, 1 (1985).
[15] H. Neumann and G. Arlt, Ferroelectrics **69**, 179 (1986).
[16] S. S. Villamil, H. Y. Lee, and L. C. Burton, IEEE Trans. Compon., Hybrids, Manuf. Technol. **12**, 482 (1987).
[17] H. Y. Lee, S. S. Villamil, and L. C. Burton, in *Proceedings of the 6th IEEE International Symposium on Applications of Ferroelectrics* (Lehigh University, Bethlehem, PA, 1986), p. 361.
[18] H. Y. Lee and L. C. Burton, IEEE Trans. Compon., Hybrids, Manuf. Technol. **9**, 469 (1986).
[19] R. Waser, in *Proceedings of the 1st Conference of the European Ceramic Society* (Maastricht, 1989).
[20] Y.-M. Chiang and T. Takagi, J. Am. Ceram. Soc. **73**, 3278 (1990).
[21] R. Waser and D. M. Smyth, *Ferroelectric Thin Films: Synthesis and Basic Properties* (Gordon and Breach, New York, 1994), p. 47.
[22] M. Vollmann and R. Waser, J. Electroceram. **1**, 51 (1997).
[23] R. Waser, T. Baiatu, and K. H. Härdtl, J. Am. Ceram. Soc. **73**, 1663 (1990).
[24] R. Waser, J. Am. Ceram. Soc. **74**, 1934 (1991).
[25] R. Hagenbeck and R. Waser, in *Proceedings of the 4th International Conference on Electronic Ceramics and Applications* (Augustinus Verlag, Aachen, 1994), p. 647.
[26] R. Hagenbeck, L. Schneider-Störmann, M. Vollmann, and R. Waser, Mater. Sci. Eng., B **39**, 179 (1996).
[27] R. Hagenbeck, Ph.D. thesis (in German), RWTH Aachen, 1998.
[28] M. Vollmann, R. Hagenbeck, and R. Waser, J. Am. Ceram. Soc. **80**, 2301 (1997).
[29] J. Jamnik and J. Maier, J. Electrochem. Soc. **145**, 1762 (1998).
[30] J. Jamnik and J. Maier, J. Phys. Chem. Solids **59**, 1555 (1998).
[31] J. Jamnik and J. Maier, Solid State Ionics **119**, 191 (1999).
[32] J. Fleig and J. Maier, J. Eur. Ceram. Soc. **19**, 693 (1999).
[33] J. Fleig, Solid State Ionics **131**, 117 (2000).
[34] J. Fleig, S. Rodewald, and J. Maier, J. Appl. Phys. **87**, 2372 (2000).
[35] S. Rodewald, J. Fleig, and J. Maier, J. Am. Ceram. Soc. **84**, 521 (2001).
[36] R. Waser, *Ferroelectric Ceramics* (Birkhäuser Verlag, Basel, 1993), p. 273.
[37] F. A. Kröger and H. J. Vink, in *Solid State Physics*, edited by F. Seitz and D. Turnbull (Academic Press, New York, 1956), p. 307.
[38] N.-H. Chan and D. M. Smyth, J. Electrochem. Soc. **123**, 1584 (1976).
[39] N.-H. Chan, R. K. Sharma, and D. M. Smyth, J. Am. Ceram. Soc. **64**, 556 (1981).
[40] D. M. Smyth, Solid State Chem. **15**, 145 (1984).
[41] C. Tragut and K. H. Härdtl, Sens. Actuators B **4**, 425 (1991).
[42] T. Bieger, J. Maier, and R. Waser, Sens. Actuators B **7**, 763 (1992).
[43] R. Waser, J. Am. Ceram. Soc. **74**, 1934 (1991).
[44] M. Fleischer, H. Meixner, and C. Tragut, J. Am. Ceram. Soc. **75**, 1666 (1992).
[45] R. Moos, Ph.D. thesis (in German), University of Karlsruhe, 1994.
[46] I. Denk, W. Münch, and J. Maier, J. Am. Ceram. Soc. **78**, 3265 (1995).
[47] R. Moos and K. H. Härdtl, J. Am. Ceram. Soc. **80**, 2549 (1997).
[48] M. L. Mecartney, R. Sinclair, and G. J. Ewell, Adv. Ceram. **1**, 207 (1980).
[49] R. Hagenbeck and R. Waser, J. Appl. Phys. **83**, 2083 (1998).
[50] N. Söylemezoglu, Diploma thesis (in German), RWTH Aachen, 2001.
[51] H. P. Langtangen, *Computational Partial Differential Equations* (Springer, Berlin, 1999).
[52] T. Hölbling and R. Waser (unpublished).
[53] G. E. Pike and C. H. Seager, J. Appl. Phys. **50**, 3414 (1979).
[54] M. Vollmann, Ph.D. thesis (in German) RWTH Aachen, 1997.

Downloaded 15 Dec 2006 to 134.94.122.39. Redistribution subject to AIP license or copyright, see http://jap.aip.org/jap/copyright.jsp